



**SOLUTION TO THE EULERIAN EQUATIONS BY
THE FINITE ELEMENT METHOD WITH AN
APPLICATION TO TRANSONIC FLOW**

**ENGINE TEST FACILITY
ARNOLD ENGINEERING DEVELOPMENT CENTER
AIR FORCE SYSTEMS COMMAND
ARNOLD AIR FORCE STATION, TENNESSEE 37389**

August 1976

Final Report for Period November 1974 — November 1975

Approved for public release; distribution unlimited.

Prepared for

**DIRECTORATE OF TECHNOLOGY (DY)
ARNOLD ENGINEERING DEVELOPMENT CENTER
ARNOLD AIR FORCE STATION, TENNESSEE 37389**

NOTICES

When U. S. Government drawings specifications, or other data are used for any purpose other than a definitely related Government procurement operation, the Government thereby incurs no responsibility nor any obligation whatsoever, and the fact that the Government may have formulated, furnished, or in any way supplied the said drawings, specifications, or other data, is not to be regarded by implication or otherwise, or in any manner licensing the holder or any other person or corporation, or conveying any rights or permission to manufacture, use, or sell any patented invention that may in any way be related thereto.

Qualified users may obtain copies of this report from the Defense Documentation Center.

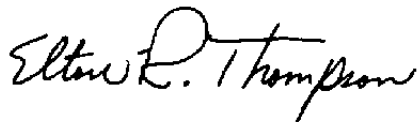
References to named commercial products in this report are not to be considered in any sense as an endorsement of the product by the United States Air Force or the Government.

This report has been reviewed by the Information Office (OI) and is releasable to the National Technical Information Service (NTIS). At NTIS, it will be available to the general public, including foreign nations.

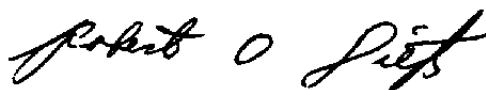
APPROVAL STATEMENT

This technical report has been reviewed and is approved for publication.

FOR THE COMMANDER



ELTON R. THOMPSON
Research & Development
Division
Directorate of Technology



ROBERT O. DIETZ
Director of Technology

UNCLASSIFIED

REPORT DOCUMENTATION PAGE		READ INSTRUCTIONS BEFORE COMPLETING FORM
1 REPORT NUMBER AEDC-TR-76-86	2 GOVT ACCESSION NO	3 RECIPIENT'S CATALOG NUMBER
4 TITLE (and Subtitle) SOLUTION TO THE EULERIAN EQUATIONS BY THE FINITE ELEMENT METHOD WITH AN APPLICATION TO TRANSONIC FLOW		5 TYPE OF REPORT & PERIOD COVERED Final Report - November 1974 - November 1975
7 AUTHOR(s) W. J. Phares and K. R. Kneile, ARO, Inc.		6 PERFORMING ORG REPORT NUMBER
9 PERFORMING ORGANIZATION NAME AND ADDRESS Arnold Engineering Development Center(DY) Air Force Systems Command Arnold Air Force Station, Tennessee 37389		8 CONTRACT OR GRANT NUMBER(s)
11 CONTROLLING OFFICE NAME AND ADDRESS Arnold Engineering Development Center (DYFS) Arnold Air Force Station, Tennessee 37389		10 PROGRAM ELEMENT, PROJECT, TASK AREA & WORK UNIT NUMBERS Program Element 65807F
14 MONITORING AGENCY NAME & ADDRESS (if different from Controlling Office)		12 REPORT DATE August 1976
		13 NUMBER OF PAGES 34
		15 SECURITY CLASS (of this report) UNCLASSIFIED
		15a DECLASSIFICATION/DOWNGRADING SCHEDULE N/A
16 DISTRIBUTION STATEMENT (of this Report) Approved for public release; distribution unlimited.		
17 DISTRIBUTION STATEMENT (of the abstract entered in Block 20, if different from Report)		
18 SUPPLEMENTARY NOTES Available in DDC		
19 KEY WORDS (Continue on reverse side if necessary and identify by block number) mathematical analysis time (integration) equations (Eulerian) numerical results solutions (general) transonic flow steady state airfoils		
20 ABSTRACT (Continue on reverse side if necessary and identify by block number) The Eulerian equations are solved by use of the finite element method (FEM) in conjunction with the Galerkin method of weighted residuals. The unsteady, nonconservative form of the equations is used to obtain the steady-state solution. Modifica- tions are made in the time integration to improve stability at the cost of sacrificing the transient behavior. Numerical results		

UNCLASSIFIED

UNCLASSIFIED

20. ABSTRACT (Continued)

are presented which compare reasonably well with other numerical solutions and with experimental data for transonic flow over airfoils.

UNCLASSIFIED

PREFACE

The work reported herein was conducted by the Arnold Engineering Development Center (AEDC), Air Force Systems Command (AFSC), under Program Element 65807F. The results of this research were obtained by ARO, Inc. (a subsidiary of Sverdrup & Parcel and Associates, Inc.), contract operator of AEDC, AFSC, Arnold Air Force Station, Tennessee. The work was done under ARO Project Numbers R33P-60A and R33A-02A. The authors of this report were W. J. Phares and K. R. Kneife, ARO, Inc. The manuscript (ARO Control No. ARO-ETF-TR-76-30) was submitted for publication on March 10, 1976.

The authors would like to express their appreciation to C. E. Peters, ARO, Inc., who encouraged this research. Acknowledgement is also made to F. C. Loper and J. H. Fox, ARO, Inc., whose consultation was most valuable.

CONTENTS

	<u>Page</u>
1.0 INTRODUCTION	5
2.0 ANALYSIS	
2.1 General Discussion	5
2.2 Basic Equations	6
2.3 Formulation of the Elements	7
2.4 Galerkin Method of Weighed Residuals	9
2.5 Boundary Conditions	11
2.6 Calculation of Terms in the Elemental System of Equations	13
2.7 Integration in Time	14
3.0 RESULTS AND DISCUSSION	16
4.0 CONCLUDING REMARKS	17
REFERENCES	18

ILLUSTRATIONS

Figure

1. Finite Element Schematic for Flow Past a 6-percent Circular Arc Airfoil	21
2. Finite Element Schematic for Flow Past the NACA0012 Airfoil	22
3. Pressure Distribution Along the Free-Stream Axis and the 6-percent-Thick Biconvex Airfoil Chord for $M_\infty = 0.70$	23
4. Comparison of Chordwise Pressure Distributions for a 6-percent Biconvex Airfoil as a Function of Mach Number	24
5. Comparison of Chordwise Pressure Distribution for Supercritical Flow Over a 6-percent Biconvex Airfoil at $M_\infty = 0.903$	25
6. Computed Mach Number Contours for a 6-percent Biconvex Airfoil at $M_\infty = 0.903$	26

<u>Figure</u>	<u>Page</u>
7. Comparison of Chordwise Pressure Distribution over an 18-percent Biconvex Airfoil at $M_\infty = 0.741$	27
8. Comparison of Chordwise Pressure Distribution for an NACA0012 Airfoil (Ref. 6) at $M_\infty = 0.780$	28
9. Pressure Distributions for Supercritical Flow over an NACA0012 Airfoil	29
10. Chordwise Velocity Distribution for an NACA0024 Airfoil at $M_\infty = 0.2$	30

APPENDIX A

A. FINITE ELEMENT ALGORITHM FOR THE EULERIAN EQUATIONS	31
NOMENCLATURE	33

1.0 INTRODUCTION

Zienkiewicz (Ref. 1) and a number of other investigators (Refs. 2 through 5) have noted that the finite element method (FEM) is sufficiently general to be applied to a wide class of problems, including fluid mechanics. Within recent years, the FEM has been applied to the study of certain fluid mechanics problems. For example, Baker and Manhardt (Ref. 2) have applied the FEM to prediction of low-speed flows, and Chan, et al. (Ref. 5) have used the FEM in the solution of the small disturbance equation for transonic flow.

It is the purpose of this report to present results of a study of the application of the FEM to the compressible flow equations in the non-conservative Eulerian form. The flow over an airfoil in the transonic regime is a problem of current interest and was chosen to demonstrate the power of the method. The choice of the Eulerian equations as the governing equations, rather than thin airfoil theory, was made to alleviate the restriction to thin airfoils and to allow for extension to other fluid mechanics problems. Although solution to these governing equations requires a longer convergence time and additional machine storage than does solution of the one equation of small disturbance theory, this generality will be of future advantage. Choice of the non-conservative form of the governing equations was made for computational convenience as the FEM algorithm for the conservative form is more complex and requires additional calculations.

Numerical results are presented in this study for subsonic and transonic inviscid flow over two-dimensional nonlifting airfoils. The results of the predictions are compared to experimental results and to other numerical solutions.

2.0 ANALYSIS

2.1 GENERAL DISCUSSION

The Galerkin method of weighted residuals was used with the unsteady Euler equations to obtain a system of ordinary differential equations in time. The elements used in the study were parametric, bilinear quadrilateral elements (Ref. 1). During this study various difficulties were encountered with the straightforward application of

finite elements to these equations. One of the first problems encountered was the irregular behavior of the solution near the leading and trailing edges. This was caused by the discontinuity in the derivatives of the boundary. The following methods of improvement were evaluated: altering the geometry to smooth the discontinuity, enforcing stagnation conditions at these points, splitting the discontinuous boundary conditions and applying them separately to corresponding elements, and altering the functional form of the interpolation function.

Another problem encountered was instability in the time integration. Initially, an artificial viscosity term was used in an attempt to remove the instability. Steady-state solutions were obtained, but a small error was present because of the viscosity term. The next modification was the periodic altering of the solution by use of Bernoulli's equation. Although the true transient behavior was lost, the steady-state solution was obtained without using artificial viscosity for subsonic cases. In the transonic cases, while viscosity was still required, a steady-state solution could be obtained using a very small value for the viscosity. In addition to the need for the artificial viscosity term in the transonic calculations, a fine grid network in the region of the shock wave was required.

2.2 BASIC EQUATIONS

The unsteady Euler equations are

$$\begin{aligned}\rho_t^* + \rho^* u_x^* + u^* \rho_x^* + \rho^* v_y^* + v^* \rho_y^* &= 0 \\ u_t^* + u^* u_x^* + v^* u_y^* + P_x^*/\rho^* &= 0 \\ v_t^* + u^* v_x^* + v^* v_y^* + P_y^*/\rho^* &= 0\end{aligned}\tag{1}$$

The variables are nondimensionalized by

$$t = t^*/t_\infty, u = u^*/u_\infty, v = v^*/u_\infty, \rho = \rho^*/\rho_\infty, P = P^*/P_\infty, x = x^*/L, y = y^*/L$$

and

$$t_\infty = L/u_\infty$$

giving

$$\begin{aligned}\rho_t + \rho u_x + u \rho_x + \rho v_y + v \rho_y &= 0 \\ u_t + uu_x + uv_y + \frac{P_\infty}{\rho_\infty u_\infty^2} \frac{P_x}{\rho} &= 0 \\ v_t + uv_x + vv_y + \frac{P_\infty}{\rho_\infty u_\infty^2} \frac{P_y}{\rho} &= 0\end{aligned}\tag{2}$$

Using the isentropic relation in nondimensional form $P = \rho^\gamma$, Eq. (2) becomes

$$\begin{aligned}\rho_t + \rho u_x + u \rho_x + \rho v_y + v \rho_y &= 0 \\ u_t + uu_x + vu_y + \frac{\gamma P_\infty}{\rho_\infty u_\infty^2} \rho^{\gamma-2} \rho_x &= 0 \\ v_t + uv_x + vv_y + \frac{\gamma P_\infty}{\rho_\infty u_\infty^2} \rho^{\gamma-2} \rho_y &= 0\end{aligned}\quad (3)$$

The density ρ is replaced as a dependent variable with $T = \rho^{\gamma-1}$, yielding

$$T_t + (\gamma - 1)Tu_x + uT_x + (\gamma - 1)Tv_y + vT_y = 0 \quad (4a)$$

$$u_t + uu_x + vu_y + \frac{\gamma P_\infty}{(\gamma - 1)\rho_\infty u_\infty^2} T_x = 0 \quad (4b)$$

$$v_t + uv_x + vv_y + \frac{\gamma P_\infty}{(\gamma - 1)\rho_\infty u_\infty^2} T_y = 0 \quad (4c)$$

These are the equations which are used in this report. In cases where a shock occurred an artificial viscous term was needed to obtain stability. The basic equations become

$$\begin{aligned}T_t + (\gamma - 1)Tu_x + uT_x + (\gamma - 1)Tv_y + vT_y &= 0 \\ u_t + uu_x + vu_y + \frac{1}{(\gamma - 1)M_\infty^2} T_x &= \alpha \nabla^2 u \\ v_t + uv_x + vv_y + \frac{1}{(\gamma - 1)M_\infty^2} T_y &= \alpha \nabla^2 v\end{aligned}\quad (5)$$

2.3 FORMULATION OF THE ELEMENTS

The domain is divided into small quadrilateral elements, e.g., see Figs. 1 and 2. Two numbering systems are used. One is a global system which assigns a sequential node number to each node in the domain.

The method used to assign the global system will not affect the results but is a significant factor in computational efficiency. The other is an elemental system where the four nodes of each element are sequentially assigned within each element. The order used by the authors was counterclockwise starting with the lower left node. Throughout this report the numbering system used will be evident by the presence of an upper limit of 4 or N. Within each element, the variables are approximated as a function of the values at the four nodes (corners) in the following parametric form (Ref. 1):

$$\begin{aligned}
 u &= \sum_{i=1}^4 u_i \Omega^i(\xi, \eta) \\
 v &= \sum_{i=1}^4 v_i \Omega^i(\xi, \eta) \\
 T &= \sum_{i=1}^4 T_i \Omega^i(\xi, \eta) \\
 x &= \sum_{i=1}^4 x_i \Omega^i(\xi, \eta) \\
 y &= \sum_{i=1}^4 y_i \Omega^i(\xi, \eta)
 \end{aligned} \tag{6}$$

where $(-1 \leq \xi \leq 1 \text{ and } -1 \leq \eta \leq 1)$ and

$$\begin{aligned}
 \Omega^1 &= (1 + \xi)(1 + \eta)/4 \\
 \Omega^2 &= (1 - \xi)(1 + \eta)/4 \\
 \Omega^3 &= (1 - \xi)(1 - \eta)/4 \\
 \Omega^4 &= (1 + \xi)(1 - \eta)/4
 \end{aligned} \tag{7}$$

The dependent variables can therefore be approximated over the entire domain as a linear combination of values given at the nodes.

Partial derivatives within an element may be obtained from Eqs. (6) and (7) as follows. Consider for example

$$u_x = u_\xi \xi_x + u_\eta \eta_x$$

where

$$\xi_x = y_\eta / J \quad , \quad \eta_x = -y_\xi / J$$

$$J = x_\xi y_\eta - x_\eta y_\xi$$

giving

$$\begin{aligned} u_x &= \left(u_\xi y_\eta - u_\eta y_\xi \right) / J \\ &= \sum_{i=1}^4 u_i \left(\Omega_\xi^i \sum_{k=1}^4 y_k \Omega_\eta^k - \Omega_\eta^i \sum_{k=1}^4 y_k \Omega_\xi^k \right) / \\ &\quad \left(\sum_{k=1}^4 x_k \Omega_\xi^k \sum_{k=1}^4 y_k \Omega_\eta^k - \sum_{k=1}^4 x_k \Omega_\eta^k \sum_{k=1}^4 y_k \Omega_\xi^k \right) \end{aligned} \quad (8)$$

Thus the partial derivatives are a linear combination of the nodal values. It is noted that while the dependent variables are continuous between elements, the partial derivatives are discontinuous at the boundaries.

The time derivatives are treated as follows:

$$\begin{aligned} u_t &= \sum_{i=1}^4 \dot{u}_i \Omega^i \\ v_t &= \sum_{i=1}^4 \dot{v}_i \Omega^i \\ T_t &= \sum_{i=1}^4 \dot{T}_i \Omega^i \end{aligned} \quad (9)$$

2.4 GALERKIN METHOD OF WEIGHTED RESIDUALS

Substituting the approximations given by Eq. (6) into Eq. (4) for each element in the domain gives equations of the following form:

$$\begin{aligned} \sum_{i=1}^N a_i \dot{T}_i &= F_1(T_j, u_j, v_j) \\ \sum_{i=1}^N a_i \dot{u}_i &= F_2(T_j, u_j, v_j) \\ \sum_{i=1}^N a_i \dot{v}_i &= F_3(T_j, u_j, v_j) \quad , \quad j = 1, 2, 3, \dots, N \end{aligned} \quad (10)$$

where α_i and F_i are implicit functions of the independent variables x and y over the domain. The above consists of three continuum sets of equations with a finite (three times the number of node points) number of unknowns. Since all of the implied equations cannot be satisfied, a selected set of weighted integrals of these equations was chosen:

$$\int_R \phi_k \sum_{i=1}^N \alpha_i \dot{T}_i dA = \int_R F_1(T_j, u_j, v_j) \phi_k dA \quad (11a)$$

$$\int_R \phi_k \sum_{i=1}^N \alpha_i \dot{u}_i dA = \int_R F_2(T_j, u_j, v_j) \phi_k dA \quad (11b)$$

$$\int_R \phi_k \sum_{i=1}^N \alpha_i \dot{v}_i dA = \int_R F_3(T_j, u_j, v_j) \phi_k dA \quad (11c)$$

where $j, k = 1, 2, \dots, N$

The ϕ_k 's are the basis functions formed from the elemental Ω 's. There is a basis function associated with each global node, such that the function is unity at this node and zero at all other nodes. The basis function is a composite of the elemental Ω 's as follows. For a point in the domain that lies in an element containing the k^{th} node, the value of ϕ_k is defined as the value of the Ω in that element which has a unit value at the k^{th} node. The term ϕ_k is defined as zero at all other points.

In actual calculations the integration represented in Eq. (11) is done separately for each element and then assembled to form the equations. When the integration is performed over a single element only four basis functions will give nonzero results. Within this element these four basis functions are identical to the four interpolation functions $\Omega^1, \Omega^2, \Omega^3$, and Ω^4 . The elemental system is therefore defined as

$$\begin{aligned} \int_{R_m} \Omega^j \sum_{i=1}^4 b_i \dot{T}_i dA &= \int_{R_m} G_1(T_j, u_j, v_j) \Omega^j dA \\ \int_{R_m} \Omega^j \sum_{i=1}^4 b_i \dot{u}_i dA &= \int_{R_m} G_2(T_j, u_j, v_j) \Omega^j dA \\ \int_{R_m} \Omega^j \sum_{i=1}^4 b_i \dot{v}_i dA &= \int_{R_m} G_3(T_j, u_j, v_j) \Omega^j dA \quad , \quad j = 1, 2, 3, 4 \end{aligned} \quad (12)$$

where b_i and G_i are implicit functions of the independent variables x and y over the elemental domain. The above is a system of twelve

equations in twelve unknown derivatives. A more detailed analysis of Eq. (12) is shown in Appendix A. During assembly, the elemental systems are combined to form Eq. (11). This is done by summing together corresponding elemental equations such that the Ω 's in Eq. (12) form the ϕ_k 's in Eq. (11). At the same time, terms that correspond to the same unknown are combined, enforcing continuity between elements. This assembly process converts the individual elemental system of Eq. (12) into the global system given by Eq. (11).

2.5 BOUNDARY CONDITIONS

The examples used in this report are flow around nonlifting two-dimensional airfoils. The boundary conditions for these problems are as follows. Consider Fig. 1 with the top boundary a far-removed wall and the upstream and downstream boundaries being sufficiently removed to assume free-stream conditions at these boundaries. The boundary conditions are

$$\begin{aligned} u = 1, T = 1, v = 0 & \quad \text{at the upstream and downstream boundaries} \\ v = 0 & \quad \text{at the upper boundary and along the centerline} \\ v = u \tan \theta & \quad \text{along the airfoil} \end{aligned} \quad (13)$$

The boundary conditions are applied in time derivative form; that is, Eq. (13) is differentiated with respect to time, obtaining

$$\dot{u} = \dot{v} = \dot{T} = 0 \quad \text{at the upstream and downstream boundaries} \quad (14a)$$

$$\dot{v} = 0 \quad \text{at the upper boundary along the centerline} \quad (14b)$$

$$\dot{v} = \dot{u} \tan \theta \quad \text{along the airfoil} \quad (14c)$$

If Eq. (13) is satisfied for the initial conditions, then Eq. (14) will enforce Eq. (13) for all time.

When Eq. (14a) is applied to a node, the corresponding equation from Eq. (11b) is removed from the system. Likewise when Eq. (14b) is applied at a node, a corresponding equation from Eq. (11c) is removed. In the case of Eq. (14c), the equations in Eqs. (11b) and (11c) are replaced by Eq. (14c) and a corresponding linear combination from Eqs. (11b) and (11c). The linear combination is based on the geometry at the point and is of the form

$$(\text{Eq. 11b}) + \tan \theta (\text{Eq. 11c})$$

The points at the leading and trailing edges require special handling in order to treat the discontinuity of the slopes at these points. At these points the boundary conditions are applied to the elemental equations that form Eq. (11) before assembling. In this manner, a different value for the boundary condition may be applied to each side of the same point. Because of the discontinuity in slope, a discontinuity in u and v also occurs at these points.* The assembly process is altered at these points to enforce continuity of T and W . The above process is easily accomplished as follows. The columns corresponding to u and v at the singular point are combined into a single W column by

$$W \text{ column} = \cos \theta (u \text{ column}) + \sin \theta (v \text{ column})$$

The rows for \dot{u} and \dot{v} at the singular point are combined into a single \dot{W} row by

$$\dot{W} \text{ row} = (\dot{u} \text{ row}) + \tan \theta (\dot{v} \text{ row})$$

The previous operations result in a new elemental system of equations with one less equation and unknown. In order to maintain a simple assembly process a dummy equation and unknown are added to the element system. This transformed elemental system is then assembled with the rest of the elemental systems. The regular boundary conditions are then applied at the other boundary nodes. When the global system is solved, the unknowns at the singular points correspond to \dot{T} , \dot{W} , and a dummy unknown that is ignored. A value for W is given at the starting time and W is integrated in time for the singular points. The velocity components at the point are obtained by using the value of $\tan \theta$ corresponding to the element under consideration. The values of u and v will be discontinuous at the singular point and along the line segment connecting the two elements. They are continuous at the other node common to both elements.

*The actual solution to the equations gives $u=v=0$ at these points with singular derivatives. Imposing $u=v=0$ as boundary conditions required either a large number of extra node points in the vicinity of the discontinuity or the inclusion of a special singular function for the fit at these points. The method described in the text gave comparable results with less computational effort.

2.6 CALCULATION OF TERMS IN THE ELEMENTAL SYSTEM OF EQUATIONS

The elemental system of Eq. (11) can be obtained in a straightforward but tedious manner. For those readers not familiar with the mechanics of the finite element method, the steps for obtaining the elemental equations for axial momentum [Eq. (4b)] will be outlined. The other two equation forms can be obtained in a similar manner.

The axial momentum Eq. (4b) when written in detail for an element is

$$\sum_{i=1}^4 u_i \Omega^i = \sum_{i=1}^4 u_i \Omega^i \sum_{j=1}^4 u_j \Omega_x^j - \sum_{i=1}^4 v_i \Omega^i \sum_{j=1}^4 u_j \Omega_y^j - K \sum_{i=1}^4 T_i \Omega_x^i \quad (15)$$

Multiplying by Ω^k and integrating over the element results in

$$\begin{aligned} \sum_{i=1}^4 u_i \int_{R_m} \Omega^i \Omega^k dA &= \sum_{i=1}^4 \sum_{j=1}^4 u_i u_j \int_{R_m} \Omega^i \Omega_x^j \Omega^k dA \\ &- \sum_{i=1}^4 \sum_{j=1}^4 v_i u_j \int_{R_m} \Omega^i \Omega_y^j \Omega^k dA - K \sum_{i=1}^4 T_i \int_{R_m} \Omega_x^i \Omega^k dA \end{aligned} \quad (16)$$

Note that while the right-hand side is a function of the dependent variables, the integrals are not; they can be evaluated on a one-time basis. This is true for the last term because T is used as a dependent variable instead of ρ . The above integrals are integrated in the parametric coordinate system (ξ, η) . The integrands are polynomials of degree three or less in either ξ or η . Consider for example the first term on the right-hand side for $i=j=k=1$:

$$\begin{aligned} \iint_{R_m} \Omega^1 \Omega_x^1 \Omega^1 dx dy &= \iint_{R_m} \Omega^1 (\Omega_\xi^1 \xi_x + \Omega_\eta^1 \eta_x) \Omega^1 dx dy \\ &= \int_{-1}^{+1} \int_{-1}^{+1} \Omega^1 [(\Omega_\xi^1 \eta_\eta - \Omega_\eta^1 \xi_\xi) J] \Omega^1 J d\xi d\eta \\ &= \int_{-1}^{+1} \int_{-1}^{+1} [(1 + \xi)(1 + \eta)/4][(1 + \eta)\eta_\eta - (1 + \xi)\xi_\xi] \\ &\quad [(1 + \xi)(1 + \eta)/4] d\xi d\eta \\ &= \int_{-1}^{+1} \int_{-1}^{+1} \frac{(1 + \xi)^2 (1 - \eta)^2}{16} [(1 + \eta)\eta_\eta - (1 + \xi)\xi_\xi] d\xi d\eta \end{aligned} \quad (17)$$

where

$$\begin{aligned} y_\eta &= y_1(1 + \xi) + y_2(1 - \xi) - y_3(1 - \xi) - y_4(1 + \xi) \\ y_\xi &= y_1(1 + \eta) - y_2(1 + \eta) - y_3(1 - \eta) + y_4(1 - \eta) \end{aligned} \quad (18)$$

The integrals are evaluated using a two-point Gaussian quadrature in each of the coordinates. By letting $k = 1, 2, 3, 4$, Eq. (16) gives four of the equations in the elemental system. The other eight are obtained from Eqs. (4a) and (4c).

Artificial viscosity terms were included at times in order to maintain stability in the transient solution. Since the magnitude of the terms was kept small, the effect on the final steady-state solution is assumed to be minor. Thus, it was assumed that an accurate evaluation of the viscous terms was not required as long as stability was maintained. The following describes the evaluation of the viscous terms as used in this report. Consider the viscous term in the axial momentum equation without the constant multiplier. Using Green's theorem results in

$$\iint_{R_m} \Omega^k \nabla^2 u \, dx dy = - \iint_{R_m} \Omega^k \cdot \nabla u \, dx dy + \oint_{\partial R_m} \Omega^k_n \cdot \nabla u \, ds$$

The line integral was ignored giving

$$\begin{aligned} - \iint_{R_m} \nabla \Omega^k \cdot \nabla u \, dA &= - \sum_{i=1}^4 \iint_{R_m} (\Omega_x^k \Omega_x^i + \Omega_y^k \Omega_y^i) \, dx dy \\ &= - \sum_{i=1}^4 u_i \int_{-1}^{+1} \int_{-1}^{+1} [(\Omega_\xi^k y_\eta - \Omega_\eta^k y_\xi)(\Omega_\xi^i y_\eta - \Omega_\eta^i y_\xi) \\ &\quad + (\Omega_x^k x_\xi - \Omega_\xi^k x_\eta)(\Omega_x^i x_\xi - \Omega_\xi^i x_\eta)] / [(x_\xi y_\eta - x_\eta y_\xi)] \, d\xi d\eta \end{aligned} \quad (19)$$

Two-point Gaussian quadrature was also used to approximate this term. The quadrature is not exact in this case because of the Jacobian in the denominator.

2.7 INTEGRATION IN TIME

Equation (11) is algebraically linear in the time derivatives. These derivatives were obtained by use of Cholesky factorization.

Since the matrix coefficients are not functions of the dependent variables, the factorization need be performed only once. The solution of the system of equations results in evaluation of the time derivatives which can be used in a numerical integration technique. The method used by the authors was fourth-order-accurate Runge-Kutta.

Initial conditions were obtained from a potential flow program. The program solved the Cauchy-Riemann equations using a finite element method. The elements used were the same in both programs. In the case of the Cauchy-Riemann equations, the resulting FEM system is a linear algebraic system which can be solved directly without iteration. The solution to the Cauchy-Riemann equations gave initial conditions for u and v . The initial conditions for T were obtained by using Bernoulli's equation in the following form:

$$T = 1 - \left(\frac{\gamma - 1}{2} \right) M_{\infty}^2 (W^2 - 1) \quad (20)$$

at each node in the flow field.

Direct numerical integration of the system gave unstable results. From observation of the transient solution, it was noticed that the dependent variable T was the first to go unstable. The integration procedure was modified to reset the variable T after a specific number of integration steps had been taken. The u and v variables from the last integration step were used in Eq. (20) to obtain the T variable for a restart. This modification will not affect the converged results since Eq. (20) is valid at steady state. For the subsonic cases, this procedure resulted in a stable convergence to the steady-state solution. The best results were obtained using about five integration steps before resetting T .

In the cases where a shock was present, the above modifications were not sufficient. For these cases an artificial viscosity term was added to the momentum equation. The viscosity term was kept as small as possible without causing an instability. Best results were obtained by systematically reducing the amount of viscosity as the solution started to converge. In these cases the steady-state conditions were recognized as a steady cyclic pattern occurring with the resetting of the initial conditions. This behavior is caused by the inconsistency between the viscous term in the momentum equation and the inviscid assumption implied in Eq. (20).

Although only the banded portion of the linear system of equations is required, the storage of these coefficients can be an obstacle for large grid networks. The linear system was modified by using only the center three diagonals; the other coefficients are set equal to zero. The resulting tridiagonal system not only required less core but resulted in faster convergence to the steady-state solution. This modification, while altering the transient solution, results in the same steady-state solution.

3.0 RESULTS AND DISCUSSION

Several selected problems have been solved in order to verify the numerical scheme discussed in previous sections. Subsonic and transonic flows over two-dimensional airfoils were investigated. The airfoils chosen were (1) a 6-percent biconvex circular arc, (2) an 18-percent biconvex circular arc, and (3) the NACA nonlifting four-digit series (NACA0012 and NACA0024) of Abbott et al. (Ref. 6).

The method was implemented on an IBM 370/165 digital computer. Storage requirements for the grid networks used in this report were 155K bytes of core. A heuristic approach was taken in determining when convergence was obtained. Integration was continued until the C_p along the center streamline held steady within plot accuracy (approximately ± 0.001 to ± 0.01 depending on the case). For subsonic cases about three minutes were required. When a shock occurred, twenty to fifty minutes were required, depending upon the strength of the shock. Several cases were run for additional time to confirm the authors' judgment in determining when steady state occurs. The final value of the artificial viscosity, α , used was the smallest value that did not give wiggles in the region ahead of the shock.

The predicted pressure distributions for various free-stream Mach numbers have been correlated with experimental data and with available numerical solutions. Figure 3 shows the predicted pressure distribution along the axis and over a 6-percent circular-arc airfoil with a free-stream Mach number, M_∞ , of 0.7. A summary of predicted pressure distributions, compared to the experimental data of Collins and Krupp (Ref. 7) and Knechtel (Ref. 8) for three subcritical free-stream Mach numbers ($M_\infty = 0.710$, 0.809 , and 0.826) and a slightly supercritical case ($M_\infty = 0.857$), is shown in Fig. 4. Further increase in free-stream Mach number to $M_\infty = 0.903$ produced a supercritical case and a shock as shown in Fig. 5. For the cases where

$M_\infty = 0.857$ and 0.903 , results obtained by Murman (Refs. 9 and 10) are also shown. For the lower Mach numbers the differences between the predictions are too small to show in the figure. In these supercritical cases, an artificial viscosity ($\alpha = 0.005$) is required to achieve stability, which has an effect of smearing the discontinuity (Ref. 11). The predicted shock location being upstream of Collin's data is attributed to the fixed wall.

Computed Mach number contours for the 6-percent circular-arc airfoil with $M_\infty = 0.903$ are shown in Fig. 6. The rough contours are attributed to poor plotter resolution and linear interpolation over the sparse grid shown in Fig. 1.

The case of transonic flow over an 18-percent circular-arc airfoil for $M_\infty = 0.741$ is shown in Fig. 7. The predicted pressure distribution over the airfoil is compared to the experimental data of McDevitt (Ref. 12). A very weak shock is predicted, which requires only a very small artificial viscosity ($\alpha = 0.001$) for stability.

Application of the scheme to two nonlifting airfoils of the NACA four-digit series (NACA0012 and NACA0024, Ref. 6) is shown in Figs. 8, 9, and 10. Predictions for the NACA0012 airfoil were calculated for the cases of $M_\infty = 0.72$ and $M_\infty = 0.80$. Figures 8 and 9 show the correlations of the predicted pressure distributions with the experimental data of Vidal et al. (Ref. 13). Figure 2 shows the grid used for the NACA0012 airfoil.

A low Mach number case for the NACA0024 airfoil is shown in Fig. 10 for the comparison of predicted velocity distributions with the theoretical calculations of Abbott (Ref. 6).

The grid network used for these problems is not ideal for blunt-leading-edge configurations. The wiggles present in the NACA wing solutions are stable in time and could be improved with a more refined grid network.

4.0 CONCLUDING REMARKS

The finite element method (FEM), based on the Galerkin weighted residual approach, has been used to compute flows over airfoils. This method was found to be sufficiently accurate and reasonably fast for

subsonic flow over circular-arc airfoils. However, difficulty was encountered in obtaining stability when a shock occurred in supercritical cases. In the present approach, the problem was solved through the use of an artificial viscosity. An increase in computing time and the shock-smearing effect were observed (Ref. 11). Also, the NACA airfoils with blunt leading edges gave difficulty and required larger convergence times.

This is a preliminary effort on the application of the FEM to the Euler equations in the transonic flow regime. Additional effort will be required to establish this scheme as an engineering tool for solutions of fluid-dynamic problems of the type considered. The convergence time must be reduced for supercritical cases which require an artificial viscosity. Also, in future work, the artificial viscous term should be replaced with the correct viscous term and the energy equation should be added to the system.

REFERENCES

1. Zienkiewicz, O. C. The Finite Element Method in Engineering Science. McGraw-Hill, London, 1971.
2. Baker, A. J. and Manhardt, P. D. "The Finite Element Method in Low Speed Aerodynamics." Old Dominion University, Norfolk, Virginia, Tech Report 75-T5.
3. Bowley, Wallace W. and Prince, J. F. "Finite Element Analysis of General Fluid Flow Problems." AIAA Paper No. 71-602, June 1971.
4. Jamet, P. and Bonnerot, R. "Numerical Solution of the Eulerian Equations of Compressible Flow by a Finite Element Method Which Follows the Free Boundary and the Interfaces." Journal of Computational Physics, Vol. 18, May 1975, pp. 21-45.
5. Chan, S. T. K., Brashears, M. R., and Young, V. V. C. "Finite Element Analysis of Transonic Flow by the Method of Weighted Residuals." AIAA Paper 75-79, January 1975.
6. Abbott, Ira H. and Doenhoff, Albert E. Theory of Wing Sections. Dover Publications, Inc., New York, June 1958.
7. Collins, Donald J. and Krupp, James A. "Experimental and Theoretical Investigations in Two-Dimensional Transonic Flow." AIAA Journal, Vol. 12, No. 6, June 1974, pp. 771-778.

8. Knechtel, E. D. "Experimental Investigation at Transonic Speeds of Pressure Distributions Over Wedge and Circular-arc Airfoil Sections and Evaluation of Perforated-Wall Interference." NASA TND-15, August 1959.
9. Murman, E. M. "Computation of Wall Effects in Ventilated Transonic Wind Tunnels." AIAA Paper 72-1007, September 1972.
10. Cole, Julian D. "Modern Developments in Transonic Flow." SIAM J. Appl. Math., Vol. 29, No. 4, December 1975, pp. 763-787.
11. Grossmen B. and Moretti, G. "Time-Dependent Computation of Transonic Flows." AIAA Paper No. 70-1322, October 1970.
12. McDevitt, John B. and Lionel, L. Levy, Jr. "Transonic Flow About a Thick Circular-Arc Airfoil." AIAA Paper No. 75-878, June 1975.
13. Vidal, R. J., Catlin, P. A., and Chudyk, D. W. "Two-Dimensional Subsonic Experiments with an NACA0012 Airfoil." CALSPAN Report No. RK-5070-A-3, December 1973.

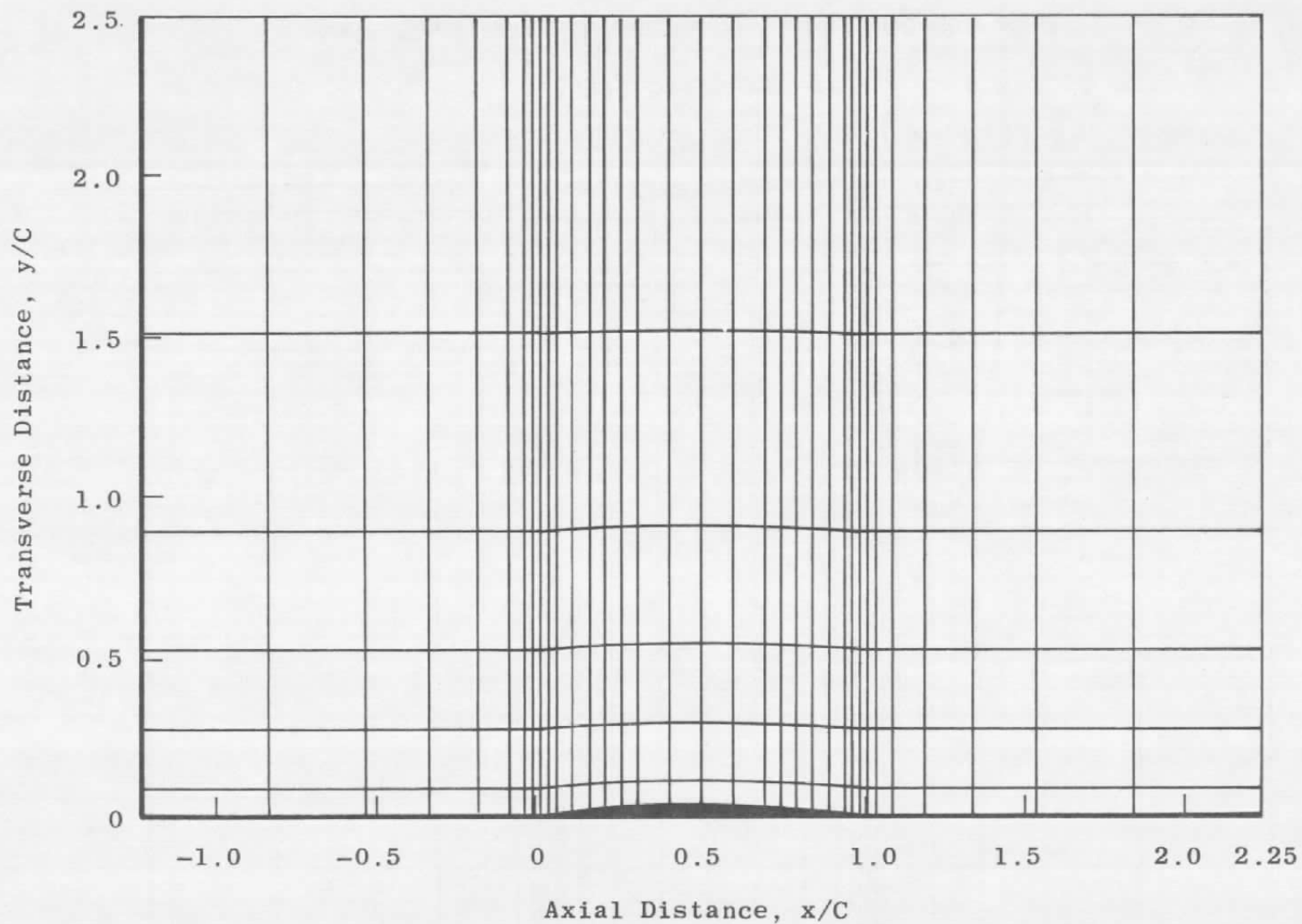


Figure 1. Finite element schematic for flow past a 6-percent circular arc airfoil.

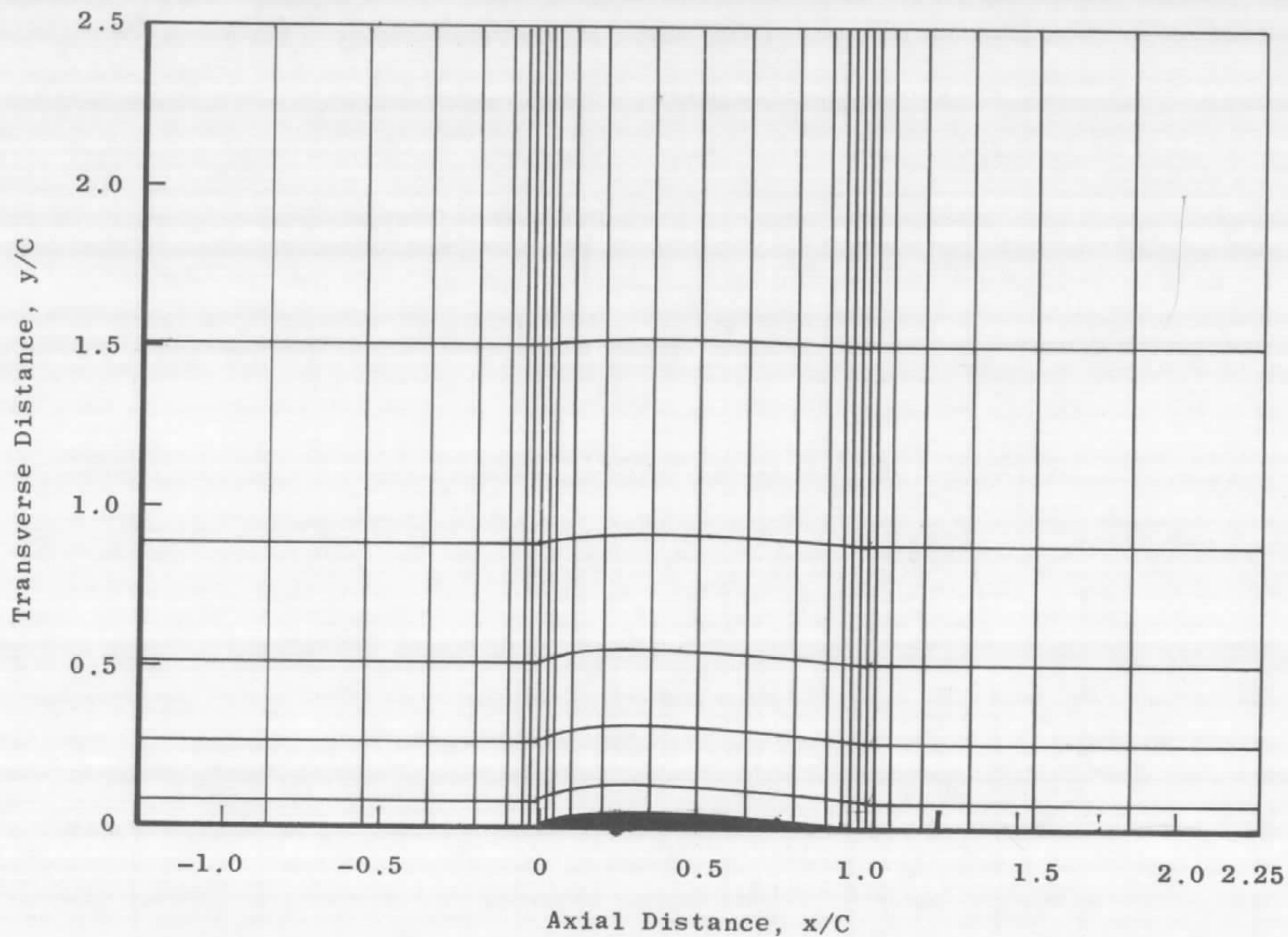


Figure 2. Finite element schematic for flow past the NACA0012 airfoil.

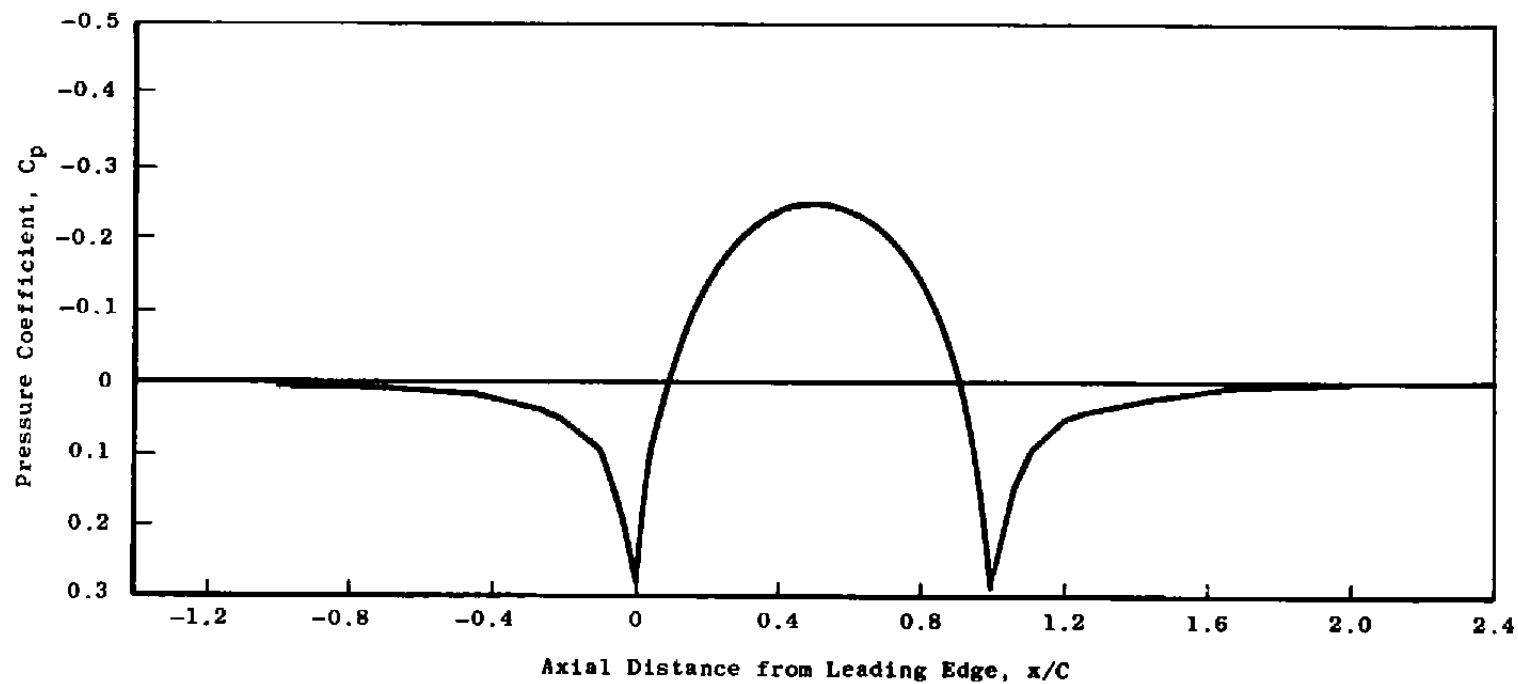


Figure 3. Pressure distribution along the free-stream axis and the 6-percent-thick biconvex airfoil chord for $M_\infty = 0.70$.

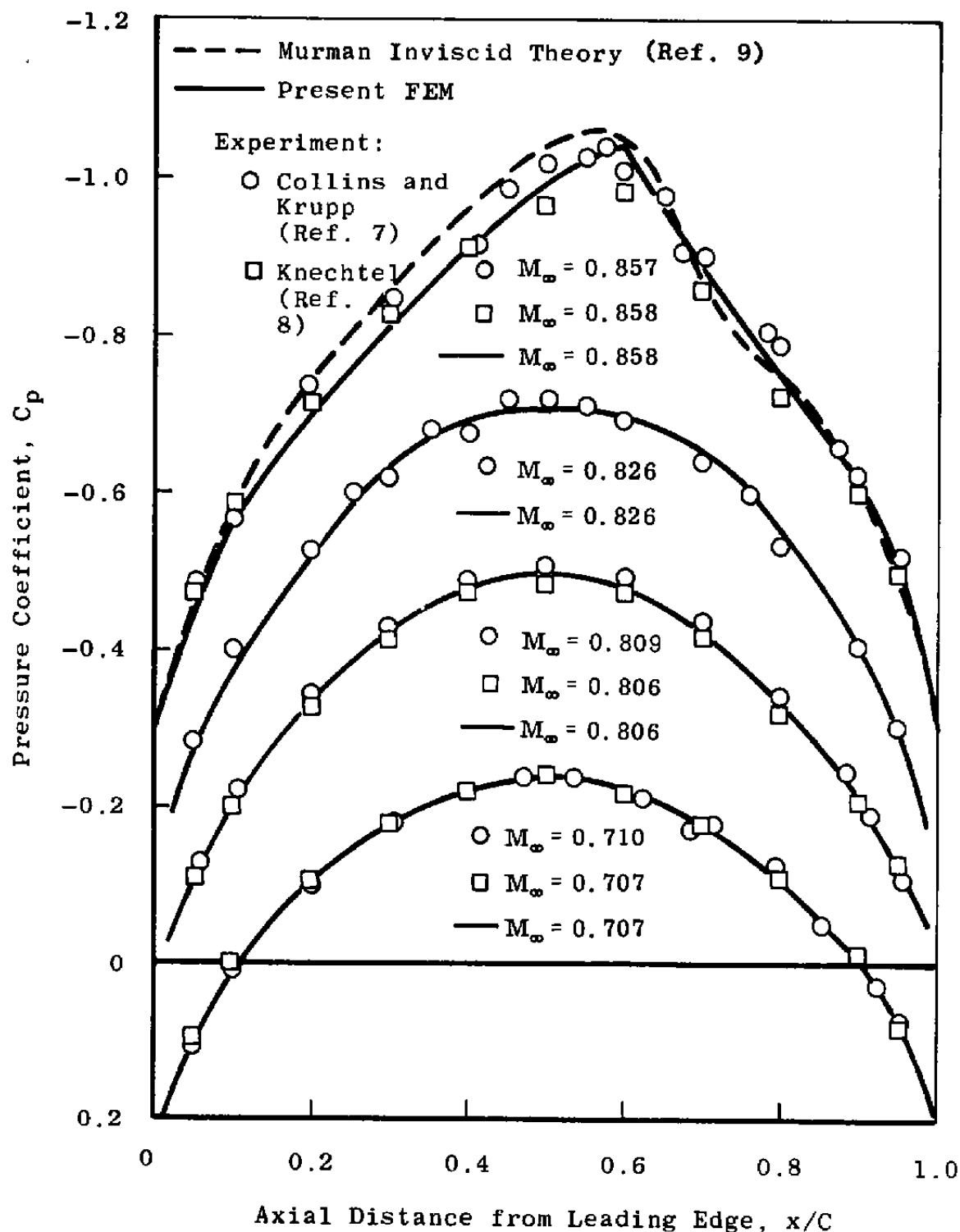


Figure 4. Comparison of chordwise pressure distributions for a 6-percent biconvex airfoil as a function of Mach number.

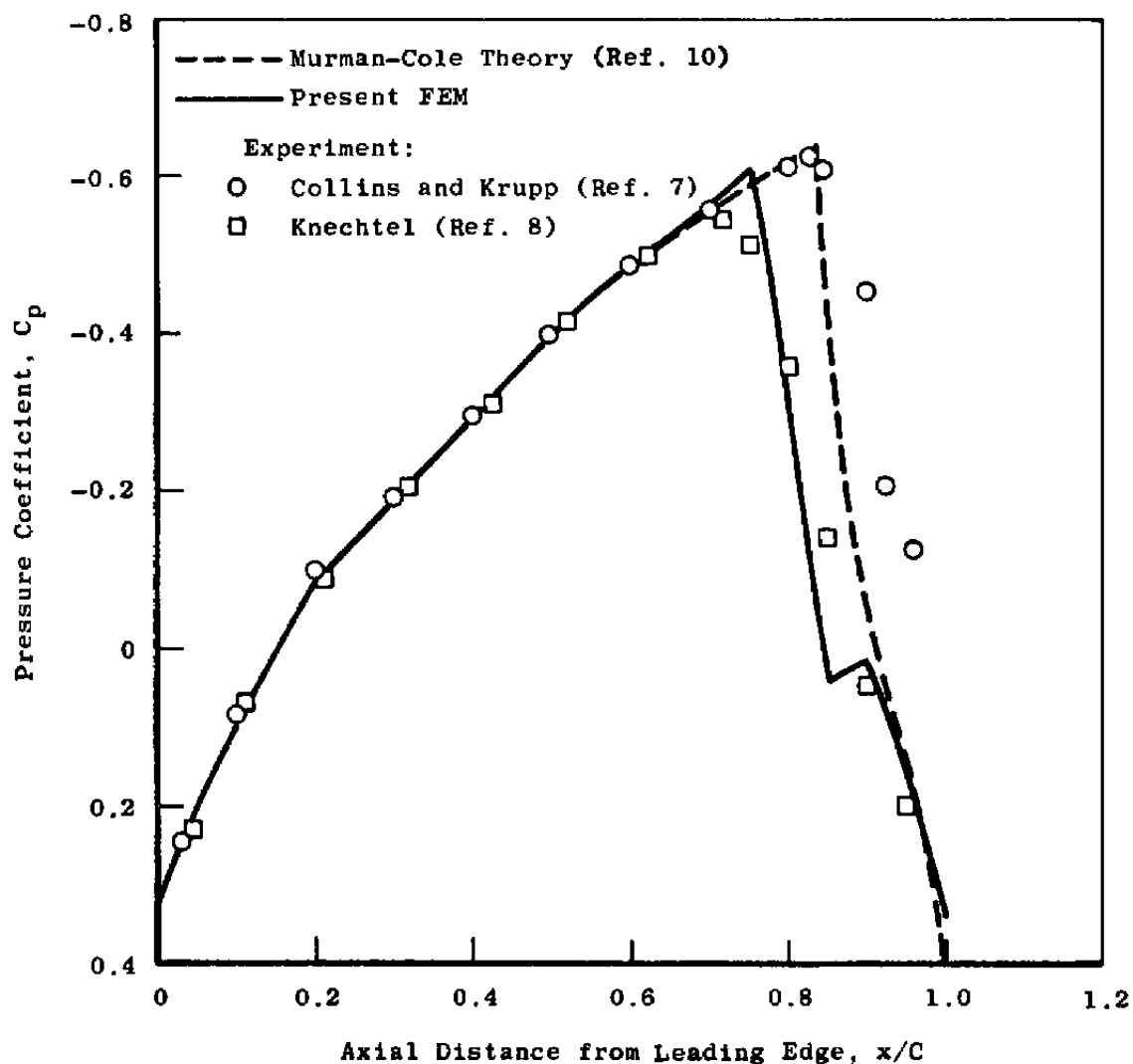


Figure 5. Comparison of chordwise pressure distribution for supercritical flow over a 6-percent biconvex airfoil at $M_\infty = 0.903$.

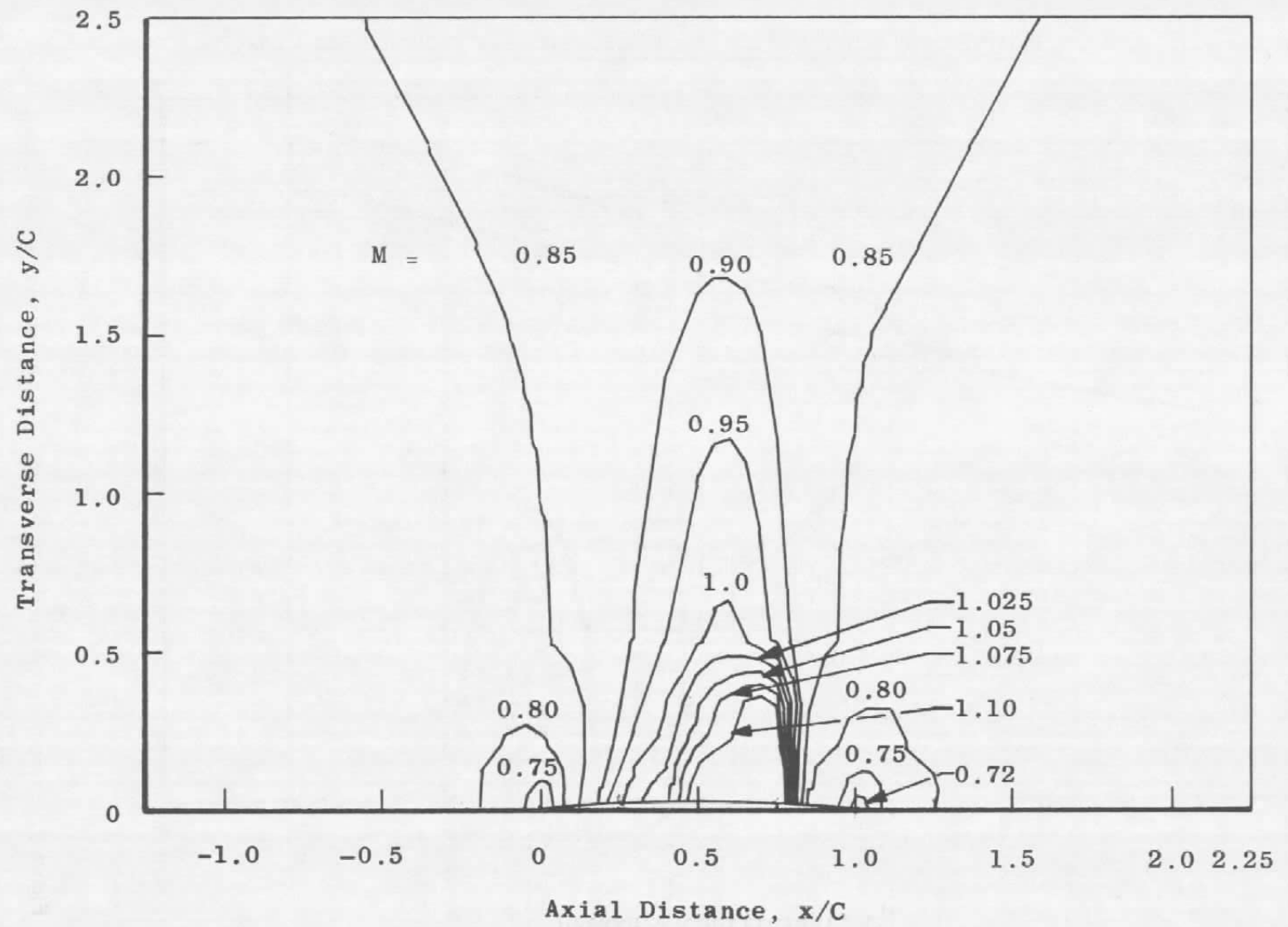


Figure 6. Computed Mach number contours for a 6-percent biconvex airfoil at $M_\infty = 0.903$.

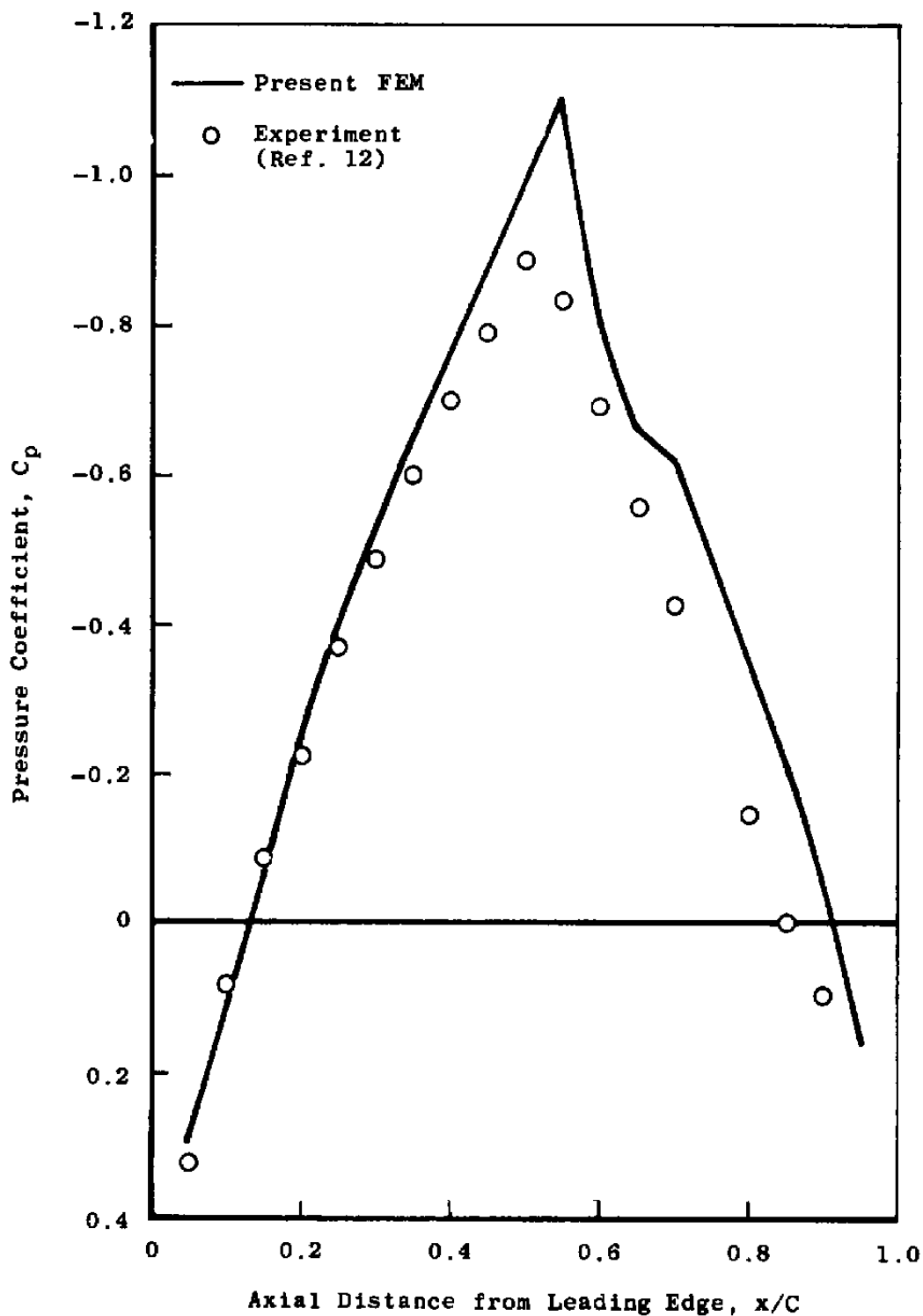


Figure 7. Comparison of chordwise pressure distribution over an 18-percent biconvex airfoil at $M_\infty = 0.741$.

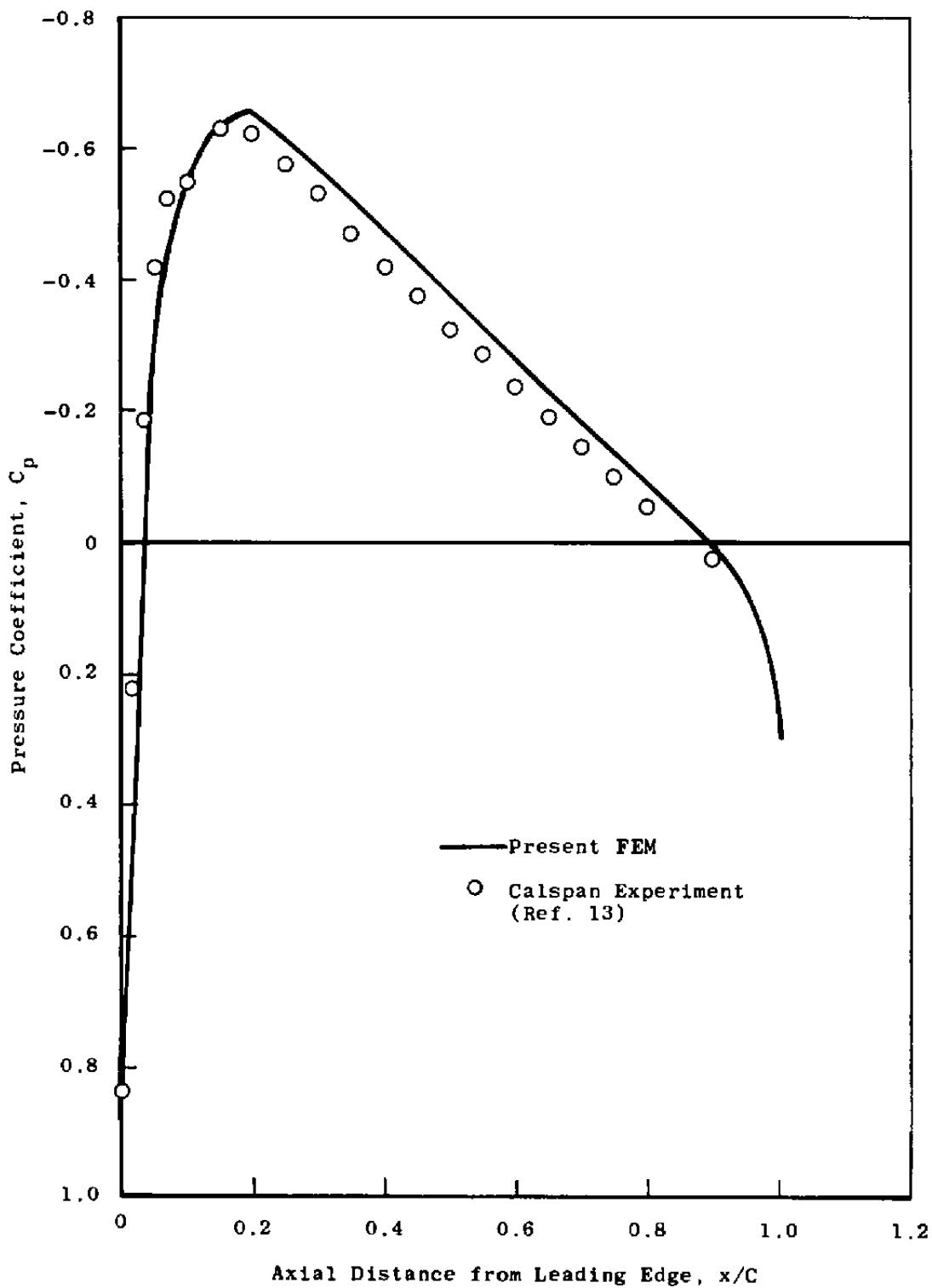


Figure 8. Comparison of chordwise pressure distribution for an NACA0012 airfoil (Ref. 6) at $M_\infty = 0.780$.

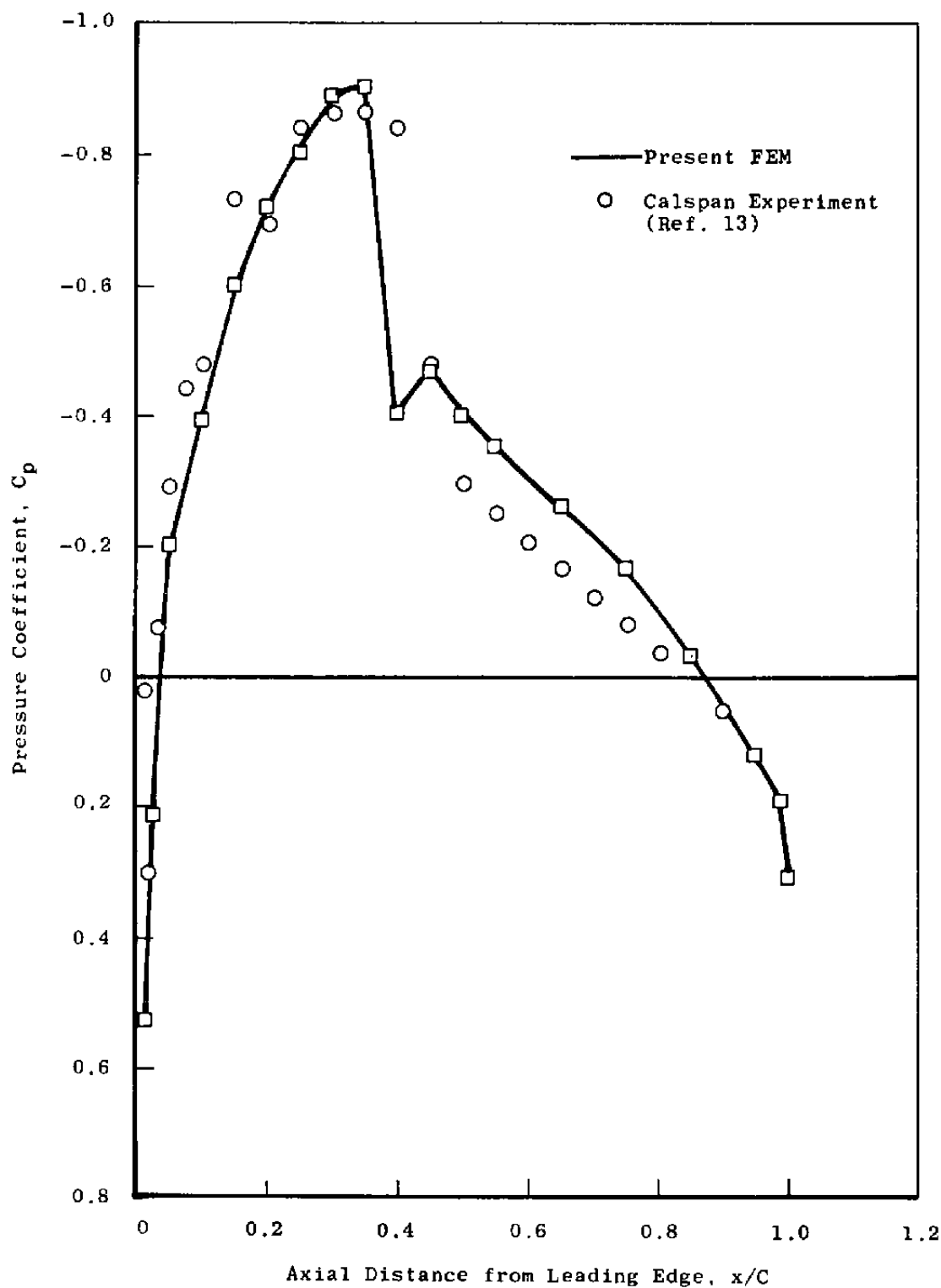


Figure 9. Pressure distributions for supercritical flow over an NACA0012 airfoil.

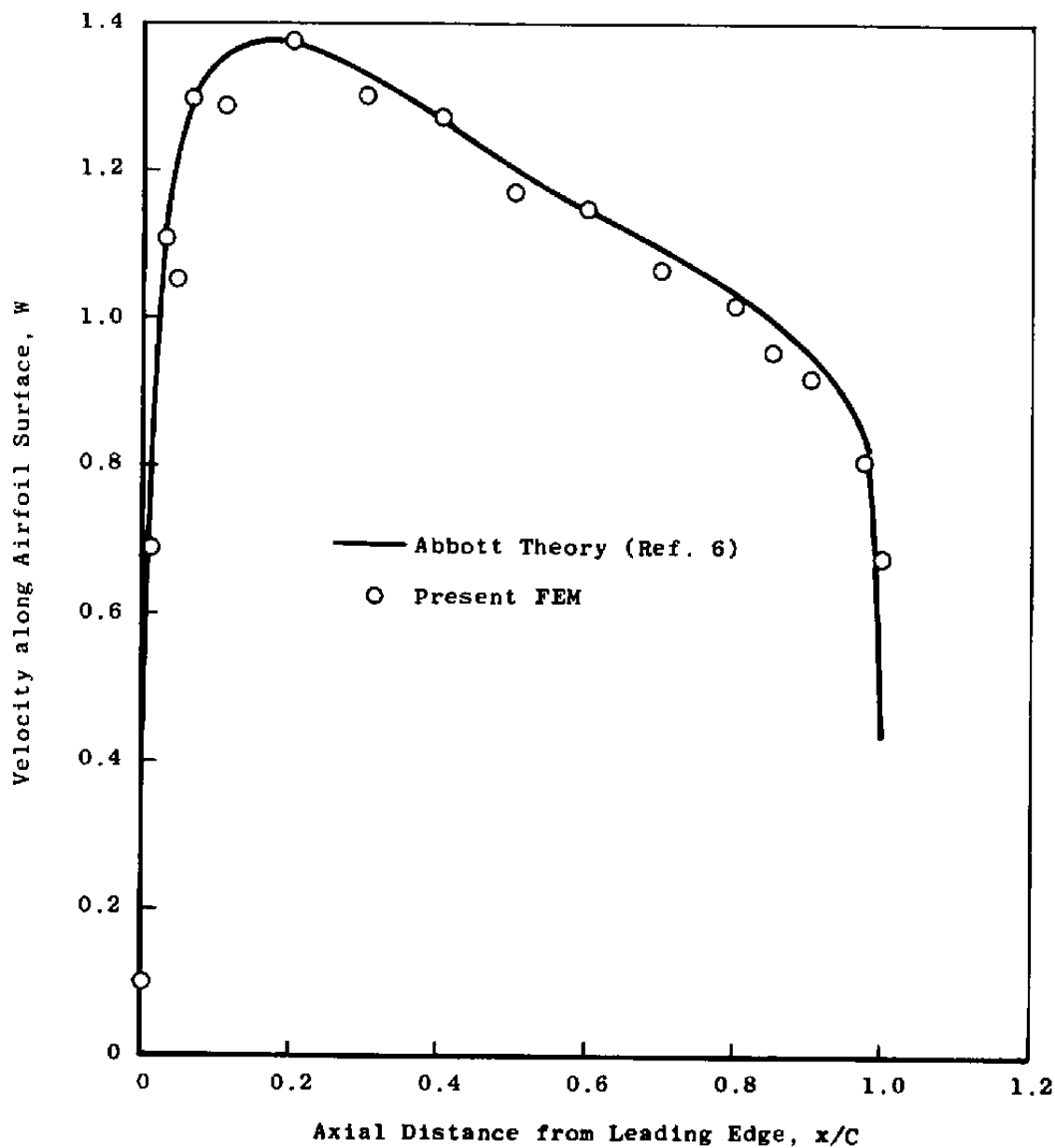


Figure 10. Chordwise velocity distribution for an NACA0024 airfoil at $M_\infty = 0.2$.

APPENDIX A

FINITE ELEMENT ALGORITHM FOR THE EULERIAN EQUATIONS

Following the scheme outlined in Section 2.0, the finite element algorithm is developed for the Eulerian equations. The Galerkin method of weighted residuals is used to obtain a system of ordinary differential equations in time.

Equation (6) is substituted into Eq. (5) and then weighted integrals are formed over the domain

$$\iint_{R_m} \left\{ \left(\sum_{i=1}^4 \Omega^i T_i \right)_t + (\gamma - 1) \sum_{i=1}^4 \Omega^i T_i \left(\sum_{i=1}^4 \Omega^i u_i \right)_x + \sum_{i=1}^4 \Omega^i u_i \left(\sum_{i=1}^4 \Omega^i T_i \right)_x + (\gamma - 1) \sum_{i=1}^4 \Omega^i T_i \left(\sum_{i=1}^4 \Omega^i v_i \right)_y + \sum_{i=1}^4 \Omega^i v_i \left(\sum_{i=1}^4 \Omega^i T_i \right)_y \right\} \Omega^k dx dy = 0 \quad (A-1a)$$

$$\iint_{R_m} \left\{ \left(\sum_{i=1}^4 \Omega^i u_i \right)_t + \sum_{i=1}^4 \Omega^i u_i \left(\sum_{i=1}^4 \Omega^i u_i \right)_x + \sum_{i=1}^4 \Omega^i v_i \left(\sum_{i=1}^4 \Omega^i u_i \right)_y + \frac{\gamma}{(\gamma - 1)M_\infty^2} \left(\sum_{i=1}^4 \Omega^i T_i \right)_x \right\} \Omega^k dx dy = \alpha \iint_{R_m} \nabla^2 \left(\sum_{i=1}^4 \Omega^i u_i \right) \Omega^k dx dy \quad (A-1b)$$

$$\iint_{R_m} \left\{ \left(\sum_{i=1}^4 \Omega^i v_i \right)_t + \sum_{i=1}^4 \Omega^i u_i \left(\sum_{i=1}^4 \Omega^i v_i \right)_x + \sum_{i=1}^4 \Omega^i v_i \left(\sum_{i=1}^4 \Omega^i v_i \right)_y + \frac{\gamma}{(\gamma - 1)M_\infty^2} \left(\sum_{i=1}^4 \Omega^i T_i \right)_y \right\} \Omega^k dx dy = \alpha \iint_{R_m} \nabla^2 \left(\sum_{i=1}^4 \Omega^i v_i \right) \Omega^k dx dy \quad (A-1c)$$

where $k = 1, 2, 3, 4$

Equation (A-1) can be rewritten as

$$\begin{aligned}
 \sum_{i=1}^4 \left(\iint_{R_m} \Omega^i \Omega^k dx dy \right) \dot{T}_i &= -(\gamma - 1) \sum_{i=1}^4 \sum_{j=1}^4 T_i u_j \iint_{R_m} \Omega^i (\Omega^j)_x \Omega^k dx dy \\
 &- \sum_{i=1}^4 \sum_{j=1}^4 T_i v_j \iint_{R_m} \Omega^j (\Omega^i)_x \Omega^k dx dy \\
 &- (\gamma - 1) \sum_{i=1}^4 \sum_{j=1}^4 T_i v_j \iint_{R_m} \Omega^i (\Omega^j)_y \Omega^k dx dy \\
 &- \sum_{i=1}^4 \sum_{j=1}^4 T_i v_j \iint_{R_m} \Omega^j (\Omega^i)_y \Omega^k dx dy
 \end{aligned} \tag{A-2a}$$

$$\begin{aligned}
 \sum_{i=1}^4 \left(\iint_{R_m} \Omega^i \Omega^k dx dy \right) \dot{u}_i &= - \sum_{i=1}^4 \sum_{j=1}^4 u_i u_j \iint_{R_m} \Omega^i (\Omega^j)_x \Omega^k dx dy \\
 &- \sum_{i=1}^4 \sum_{j=1}^4 v_i u_j \iint_{R_m} \Omega^i (\Omega^j)_y \Omega^k dx dy \\
 &- \frac{\gamma}{(\gamma - 1)M_\infty^2} \sum_{i=1}^4 T_i \iint_{R_m} (\Omega^i)_x \Omega^k dx dy
 \end{aligned} \tag{A-2b}$$

$$\begin{aligned}
 \sum_{i=1}^4 \left(\iint_{R_m} \Omega^i \Omega^k dx dy \right) \dot{v}_i &= - \sum_{i=1}^4 \sum_{j=1}^4 u_i v_j \iint_{R_m} \Omega^i (\Omega^j)_x \Omega^k dx dy \\
 &- \sum_{i=1}^4 \sum_{j=1}^4 v_i v_j \iint_{R_m} \Omega^j (\Omega^i)_y \Omega^k dx dy \\
 &- \frac{\gamma}{(\gamma - 1)M_\infty^2} \sum_{i=1}^4 T_i \iint_{R_m} (\Omega^i)_y \Omega^k dx dy
 \end{aligned} \tag{A-2c}$$

The above is a system of twelve equations in twelve unknown derivatives; the coefficients are evaluated for each element and then assembled to form Eq. (11).

NOMENCLATURE

C	Chord Length
C_p	Pressure coefficient
J	Jacobian
K	$\gamma P_\infty / ((\gamma - 1) P_\infty (u_\infty^2))$
L	Reference Length
M_∞	Free-stream Mach Number
N	Number of node points
n	Unit normal vector
P	Pressure
R	Domain
R_m	Element domain
S	Arc length
T	Temperature
t	Time
u	Axial component of velocity
$\dot{u}_i, \dot{v}_i, \dot{T}_i$	Time derivatives at the i^{th} node
V	Volume
v	Transverse component of velocity
W	$\sqrt{u^2 + v^2}$
x	Axial coordinate (measured from leading edge)
y	Transverse coordinate
α	Artificial viscosity coefficient
γ	Ratio of specific heats
θ	Body (airfoil) angle
ξ, η	Parametric coordinates
ρ	Density
ϕ	Basic functions

Ω	Interpolation function
∇	Del operator
∂R_m	Element domain boundary

SUBSCRIPTS

t	Partial derivative with respect to time
x	Partial derivative with respect to x
y	Partial derivative with respect to y
η	Partial derivative with respect to η
ξ	Partial derivative with respect to ξ
∞	Free-stream condition

SUPERSCRIPTS

$*$	Dimensional parameter
-----	-----------------------